ORIGINAL ARTICLE

Dissimilar joining of AISI 304/Q345 steels in keyhole tungsten inert gas welding process

Yifei Huang[1] · Zhen Luo[1] · Yuchen Lei[1] · Sansan Ao[1] · He Shan[1] · Yu Zhang[1]

Abstract

Keyhole tungsten inert gas welding (K-TIG) was used to join AISI 304 stainless steel with Q345 low-alloy steel of 8 mm thickness in a single pass. Welding formation and process windows in different welding speeds were discussed. Microstructure and welding properties of dissimilar joints were investigated. The results show that in a relatively high welding speed (more than 300 mm/min), high-quality weld of dissimilar steels can be obtained in the welding process window with a current of 50A. Weld microstructure is lath martensite and retained austenite. Proeutectoid ferrite and Widmanstatten structure are observed in Q345 heat-affected zone (HAZ) while no obvious grain growth is found in AISI 304 HAZ. Microhardness of the weld metal is much higher than the base metal because of the martensite structure in the weld. Tensile test was conducted with digital image correlation (DIC). The result shows that the tensile strength of the weld is almost the same as the Q345 base metal and the elongation is slightly reduced, indicating good qualities both in strength and plasticity.

Keywords Keyhole tungsten inert gas welding · AISI 304 · Low-alloy steel Q345 · Dissimilar steels · Digital image correlation (DIC)

1 Introduction

Keyhole tungsten inert gas (K-TIG) welding is an advanced method first proposed by the Australian research organization CSIRO in 1997. Compared with the traditional TIG, welding current in K-TIG is much heavier (over 300A), the arc pressure was improved, and keyhole mode welding process could be achieved as demonstrated by Jarvis and Ahmed [1, 2]. Due to the formation of keyhole in the welding process, K-TIG welding is expected to join mid-thickness workpieces in a single pass with high weld speed. Several researches have been carried out on K-TIG. Jarvis et al. studied the mechanism of keyhole formation and the influencing factors of the formation [1]. They proposed a theory that to achieve a keyhole welding process, the arc pressure should be high enough to overcome the surface tension in the weld pool plus the liquid

metal gravity. Therefore, K-TIG is an efficient method in joining low thermal conductivity materials. For materials with high thermal conductivity, the welding fusion zone is much larger and the surface tension is hard to balance liquid metal gravity, causing the weld pool to collapse. Feng et al. found that K-TIG welding can be applied to 10-mm-thick AISI 316L stainless steels without filler wire addition or edge preparation, and high-quality weld was obtained at the process window [3]. Fan et al. aimed to use K-TIG to join high-strength low-alloy steel (HSLA) with high thermal conductivity [4]. They improved the process by using a water cooling system and obtained a good formation joint with 8-mm-thick HSLA. Moreover, they compared welding in the air condition within water cooling condition by numerical simulation. Results revealed that the water cooling system was greatly helpful in reducing the width of the weld root as well as promoting surface tension, so that the liquid metal gravity can be balanced by surface tension. Another attempt in joining HSLA with K-TIG was carried out by Fang et al. [5]. By using high frequency (HF) current to join 5.5-mm-thick HSLA, a well-formed weld was obtained. Result showed that the HF promotes the arc force and improves the stability of keyhole. It is well known that joining HSLA by K-TIG has an obvious tendency to observe a collapsed keyhole because

✉ Sansan Ao
ao33@tju.edu.cn

[1] School of Materials Science and Engineering and Tianjin Key Laboratory of Advanced Joining Technology, Tianjin University, Tianjin 300072, China

Table 1 Chemical composition (wt%) of base metal

Element	C	Si	Mn	P	S	Cr	Ni	Nb	Mo	Fe
304	0.041	0.4	1.19	0.029	0.005	18.11	10.01	–	–	Bal.
Q345	0.17	0.35	1.48	0.021	0.08	0.25	0.25	0.015	0.08	Bal.

of the high thermal conductivity, and the tendency increases as thickness increases. Hence, it is still difficult to join HSLA over 8 mm thickness without any adscititious process. In summary, though the researches have made a progress, the application of K-TIG is still narrow especially in practical industry.

With the development of oil pipeline industry, the demands of dissimilar steels are increasing rapidly [6–9]. Dissimilar joints with HSLA and stainless steel are wildly used because they take both corrosion resistance and economy into consideration. Welding dissimilar materials is increasingly challenging because of differences in the chemical, physical, and mechanical properties of the base metals welded [10–13]. Certain amounts of researches have been carried out on the microstructure and properties of dissimilar joints; however, the feasibility and welding quality of K-TIG in dissimilar steel welding is still unknown.

In this paper, AISI 304 steel and Q345 low-alloy steel are joined by K-TIG. Welding parameters and process window are discussed to achieve a good weld formation in a single pass. Investigation of microstructure, mechanical properties, microhardness, and tensile properties is conducted to assess the quality of weld.

2 Experimental procedures

The base metals were AISI 304 stainless steel and low-alloy steel Q345, cutting into plates with a dimension of 250 × 100 × 8 mm. Chemical compositions of each material were presented in Table 1. The microstructures of the base metals were shown in Fig. 1, respectively. This figure shows that 304 stainless steel is filled with equiaxed austenite while Q345 consists of pearlite and ferrite.

A K-TIG experimental platform was shown in Fig. 2. An independent designed weld torch with cooling water was used for keyhole TIG in the experiment. A butt joint was performed with two plates fixed with fixtures to keep a zero gap. The torch was operated with DC electrode negative polarity. The shielding gas was pure argon at a flow rate of 25 L/min. The arc length was set to 2.5 mm. To evaluate the welding process, tests in different welding parameters were carried out, as listed in Table 2. Butt welding was carried out in all tests. This research was aimed to study the optimal welding parameters of dissimilar steels, and the test parameters were set in Table 2.

To observe the microstructure of the weld joints, specimens were dealt with cutting, grinding, and polishing. Because of the dissimilar material characteristics, different etchants were used to reveal the microstructure. Five percent Nital was used to etch the base metal of low-alloy steel. The weld zone and the base metal of 304 stainless steel were etched with aqua regia. The microstructural feature was observed by optical microscope (OM), X-ray diffraction (XRD), scanning electron microscope (SEM), and energy-dispersive spectroscopy (EDS).

Vickers hardness tests were carried out on the prepared specimens. The applied load was 1000 gf. Tensile tests were performed in accordance with the Chinese national standard of welding tests GB/T 2651–2008 [14], and the specimen dimensions were presented in Fig. 3. The thickness of the specimen is 8 mm, which is equal to the plate thickness. The tensile test was performed at tensile testing machine with 10 mm/min loading rate at room temperature. Additionally, a digital image correlation (DIC) system was used to analyze full-field strain in tensile test.

DIC is a non-interferometric and non-contacting optical metrology technology for full-field deformation and strain

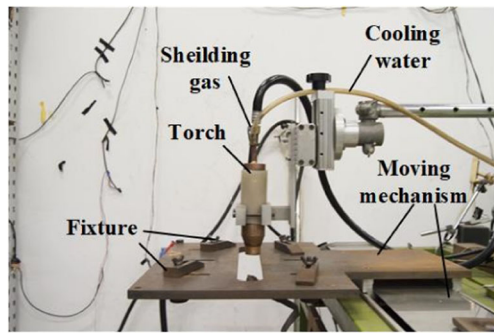**Fig. 1** Microstructure of base metal. **a** 304. **b** Q345
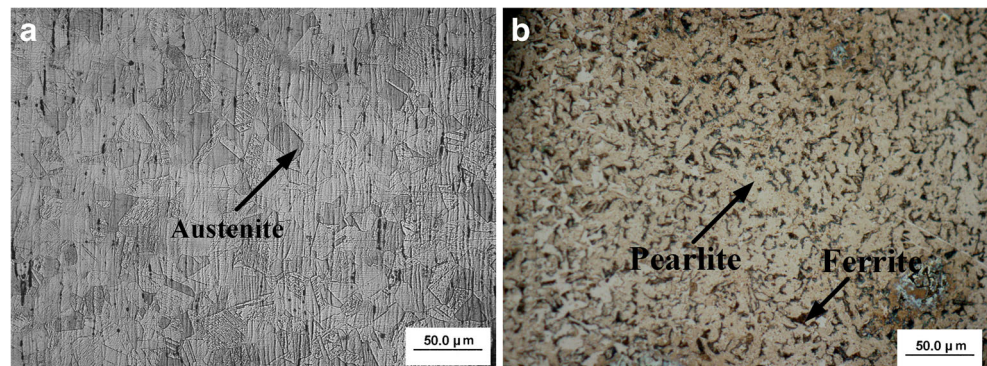
Fig. 2 K-TIG experimental platform

Table 2 Welding parameters of test

Test	Weld speed (mm/min)	Weld current (A)	Weld voltage (V)
1	300	490/510/530	16
2	350	500/520/550	16
3	400	540/570/590	16

measurements [15–17]. In this study, 2D-DIC experimental platform was established as shown in Fig.4. Specimen for tensile test was polished and painted with speckles, and a high-speed camera was prepared to record speckle behavior in testing time. Image data was stored and analyzed in a computer to show the full-field strain in tensile test. DIC was used only for weld specimens due to the interest of measuring strain at dissimilar joint area.

3 Result and discussion

3.1 Parameter effects on weld quality

The profile of the fusion zone for different welding parameters is shown in Fig. 5. Three welding speed levels of 300, 350, and 400 mm/min were tested in different welding currents, respectively. Weld cross-section profile shows a great difference in different materials. Shapes of fusion lines in 304 side are nail-type, with a wide upper part and a narrow bottom. However, the Q345 side fusion lines are relatively smooth. In the K-TIG welding process, a relatively high welding
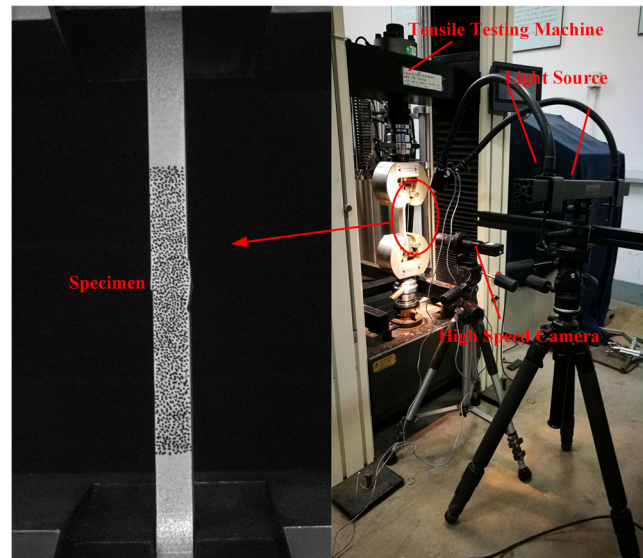

Fig. 4 Digital image correlation system

current is applied, and the arc expands. Therefore, the surface of base metals is melted in both width and depth. On the other hand, high welding current represents a large arc force, which results in the keyhole and the material melting mainly in depth. However, the thermal conductivity of Q345 is about three times than that of 304; thus, the heat input is easily conducted to the Q345 base metal so that the keyhole characteristic in Q345 side is very weak. In the 304 side, the heat input is accumulated to weld zone causing the profile similar to the keyhole heat source. Under such heating mode, both sides are different in fusion lines.

As shown in Fig. 5a, under 300 mm/min weld speed, single pass weld first formed in 490A welding current, which represents the existence of keyholes. When the test current increases, the welding process keeps stable until 530A. Weld pass slightly concaves in 530A welding current; however, all specimens in this condition are still in good shape. Further experiments show that welding formation in current above 530A is not all good. Hence, the current process window in 300 mm/min is about 490A~530A. Similar phenomenon is found in TEST 2 (350 mm/min) and TEST 3 (400 mm/min), and the current process windows are 500A~550A and 540A~590A respectively, as shown in Fig. 5b, c.
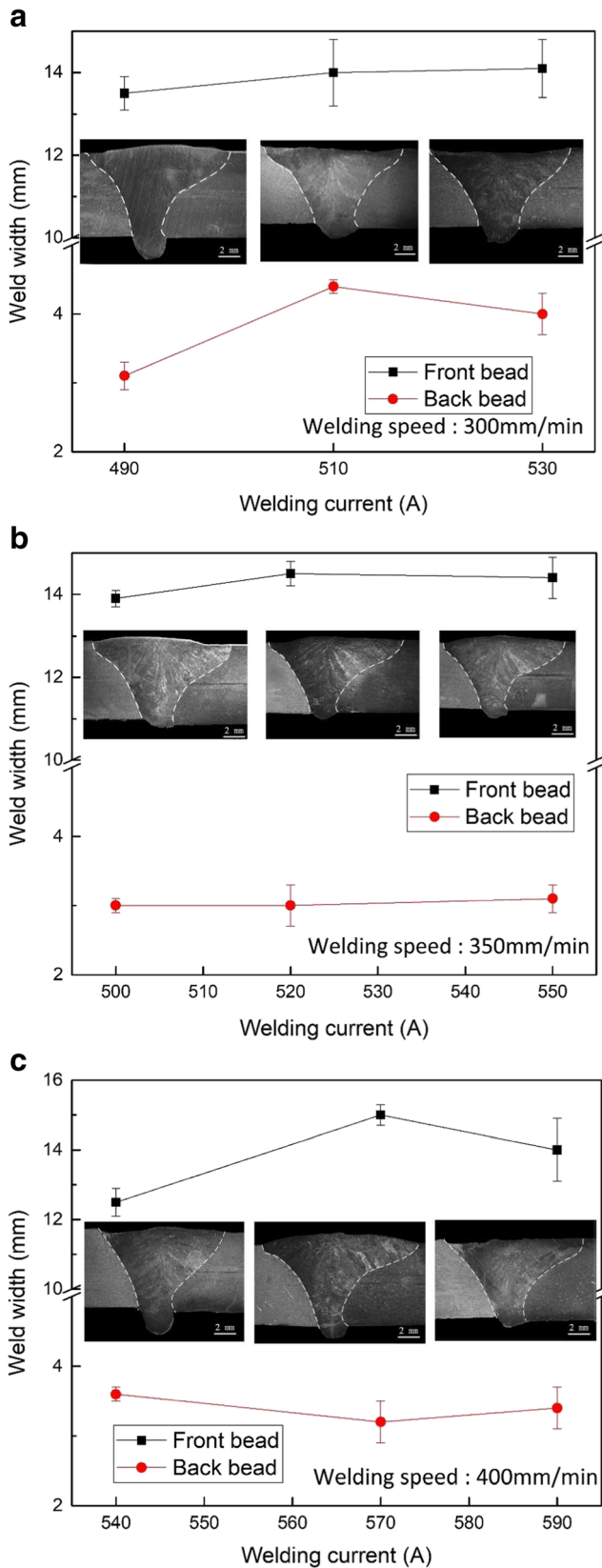
Fig. 3 Transversal tensile test specimen dimension
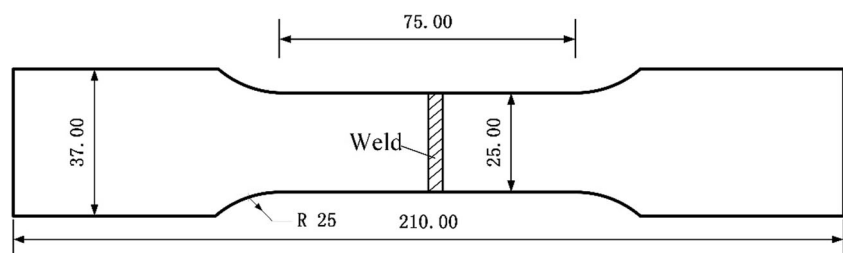
Fig. 5 Effect of welding parameter on profile of fusion zone. **a** TEST 1. **b** TEST 2. **c** TEST 3

In a specific welding speed (300 mm/min for example), functions of weld width varies with welding current are discussed. Weld width of front bead (WF) has a slightly growth trend as welding current. It can be seen that the WF (14.1 mm) at the maximum current of process window is larger than the WF (13.5 mm) at the minimum current. However, weld width of back bead (WB) represents no obvious relationship with current. All WBs are no more than 4.4 mm, because large WB will do harm to the formation of keyhole.

It should be pointed out that the joining quality of dissimilar steels by K-TIG is greatly influenced by the deviation between tungsten and center line (DTC, defined in Fig.6). Though fixtures are used to keep specimens fixed and no separation exists between two plates, unavoidably, tiny horizontal deviation—from the tungsten central axis to the contact surface of two plates—still exists as the position A or B in Fig.6. As we know, austenite is paramagnetic while ferrite is ferromagnetic; hence, the arc will be attracted to the ferrite side in joining 304 with Q345, causing a larger melting in Q345 [18]. Hence, if DTC is negative (as the position A in Fig.6), most arcs will be applied on Q345, resulting in weld pool collapse or incomplete fusion at the 304 side, based on the welding current. To obtain a high quality weld, it is of great significance to keep DTC to zero or positive (but not more than 2 mm in this paper).

3.2 Microstructure analysis

The microstructure of weld joint is shown in Fig.7a. The weld joint mainly consists of lath martensite and retained austenite. The special characteristic of lath martensite, surface relief is clearly observed. The interval of the lath is filled with bright membrane-like retained austenite. The existence of the phase is determined by analysis of XRD as shown in Fig.7b. Lath martensite structure is of high hardness and strength, and the lath boundary can impede microcrack extension. Austenite
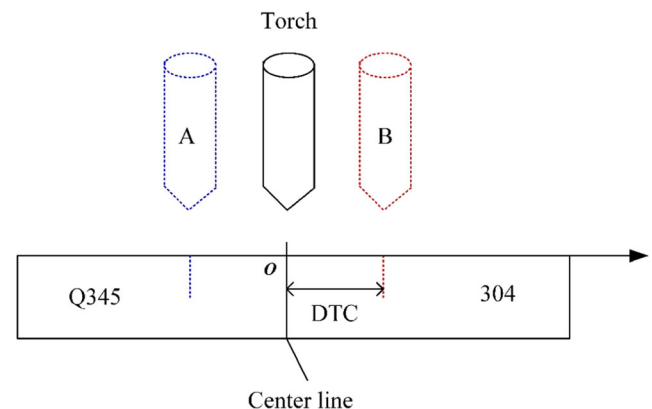

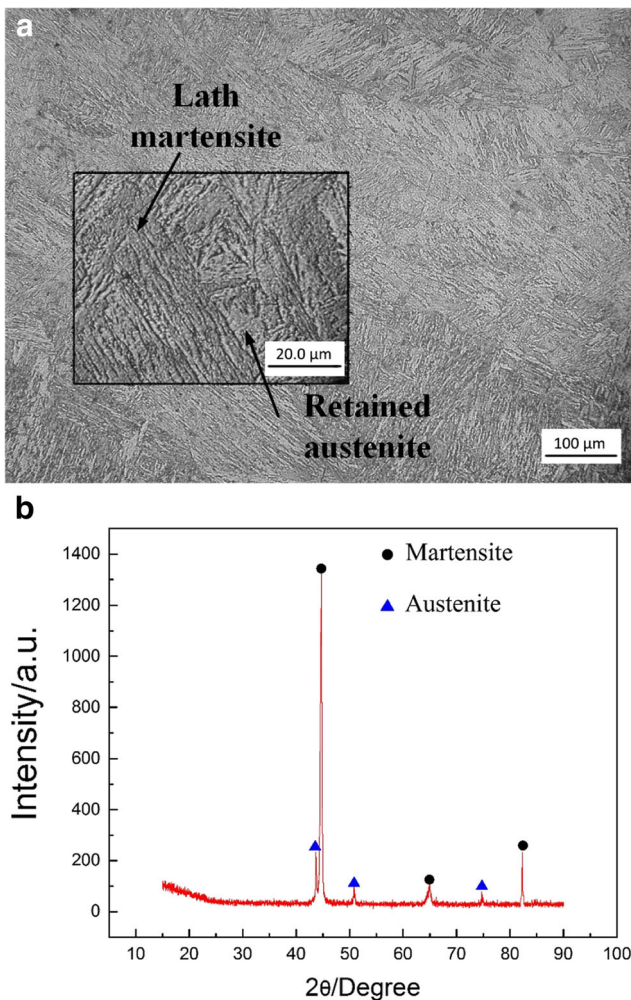Fig. 6 Illustration of deviation between tungsten and center line

Fig. 7 **a** Optical micrographs of weld metal. **b** XRD analysis of weld metal

coarse grain zone (CGZ) develops because the grain near the fusion line suffers a relatively high peak temperature in the welding process, causing austenization grain growth. Widmanstatten structure forms in CGZ as shown in Fig. 8b. Strip-like and reticulated Widmanstatten structure generates in the austenite boundary. A little far from the fusion line, the grain size is obviously decreased. The fine grain zone (FGZ) consists of recrystallization grains and proeutectoid ferrite which forms alongside the austenite boundary.

As can be seen in Fig. 8a, a type II boundary characteristic is observed close to the fusion boundary. The formation of such boundary has been attributed to the differences in the crystal structure between the materials being joined, and has been addressed in the literature for dissimilar fusion welded joints [19].

Figure 9 is the HAZ of the 304 base metal. Much worm-like texture perpendicular to welding direction is observed, because of the base metal is in rolling state [20]. Microstructure of HAZ is almost consists of austenite, and slight difference in grain size, as is shown in Fig. 9a. Different from the Q345 side, no obvious grain growth is observed near the fusion line at the 304 side. There are some reasons for the phenomenon. First, δ-ferrite phase is found in HAZ of 304, as presented in Fig. 9b, which acts as a boundary to resist the austenite grain growth. Additionally, high welding speed of K-TIG results in rapid cooling rates. And austenite structure suffers high temperature for a short time, which restrains the trend to grain growth. In summary, HAZ at 304 side is narrow by K-TIG. Similar phenomenon was also found by Kchaou et al. [21].

Figure 10 illustrates the concentration gradient of alloying elements across the interfaces. Across the Q345-WM interface in Fig. 10a, the Cr content increases stably, whereas the Fe content has a decreasing tendency. The Mn
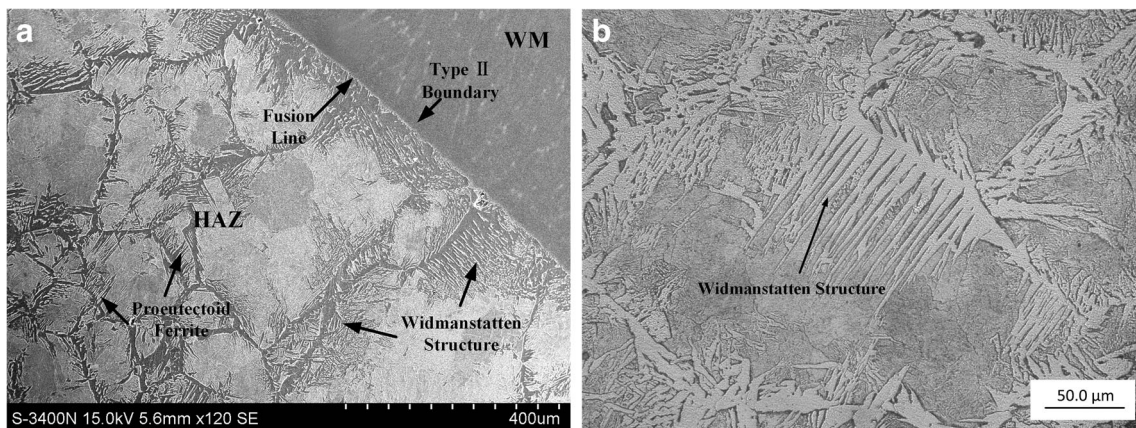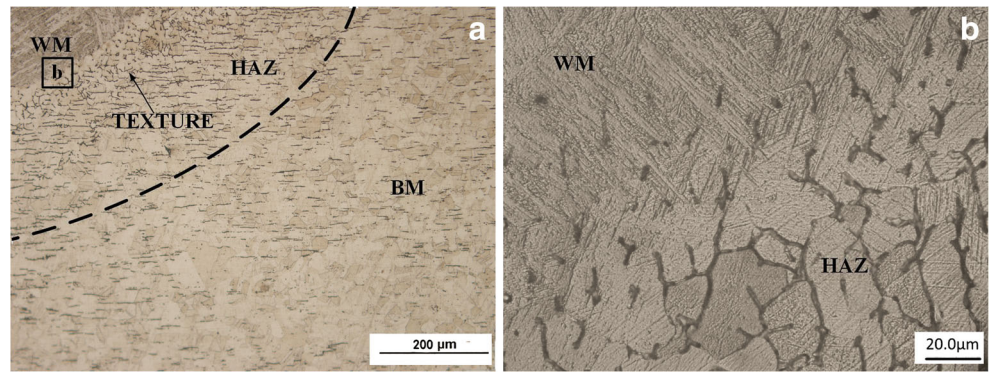
structure is of good ductility which benefits the plasticity of the weld joint.

Figure 8 shows the microstructure of HAZ at the Q345 side. Close to the fusion line, coarse grain is observed. The

Fig. 8 Microstructure of interface across Q345 to weld metal. **a** SEM micrographs of interface. **b** CGZ

Fig. 9 Microstructure of interface across 304 to weld metal. **a** HZA. **b** Interface

content and the Ni content increase slightly; however, the C content has no notable change. From Fig. 10b, the variety of elements is different. Across the WM-304 interface, the Cr and Ni contents decrease gradually, while the Fe content gains a slight promotion. The different variety tendency is caused by the distinction of BM chemical components. In the welding process, 304 stainless steels with high level of Cr and Ni content were mixed with Q345, leading to a
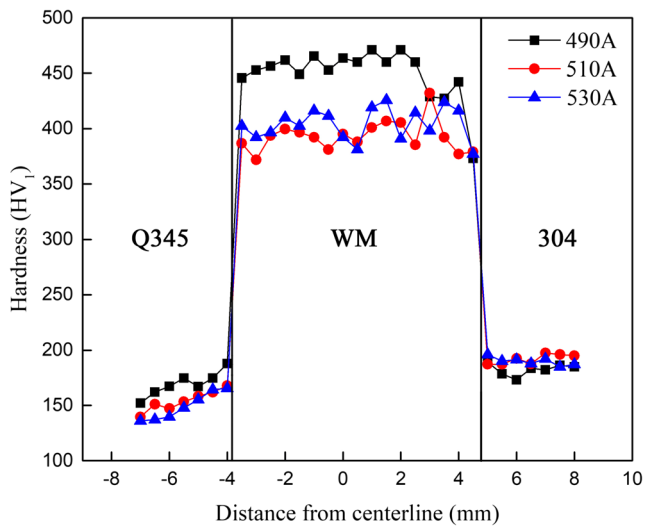
fluctuating concentration gradient. WM ingredient approximately falls in between the two BMs.

3.3 Microhardness

The Vickers hardness of the specimens in TEST 1 is shown in Fig. 11. As can be seen in Fig. 11 that trend of hardness from Q345 base metal to 304 base metal is similar in
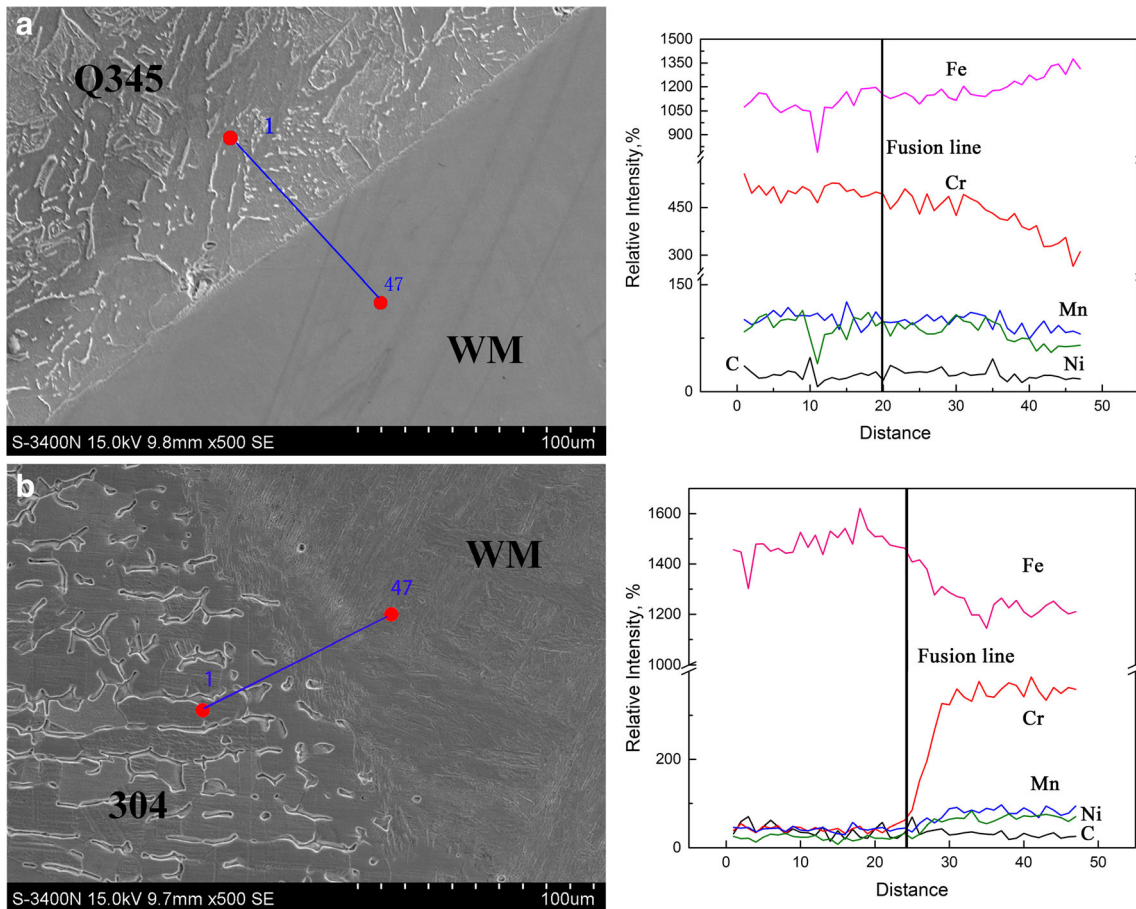
Fig. 10 EDS line scan across the interfaces. **a** WM-304 interface position and result graphs. **b** WM-Q345 interface position and result graphs
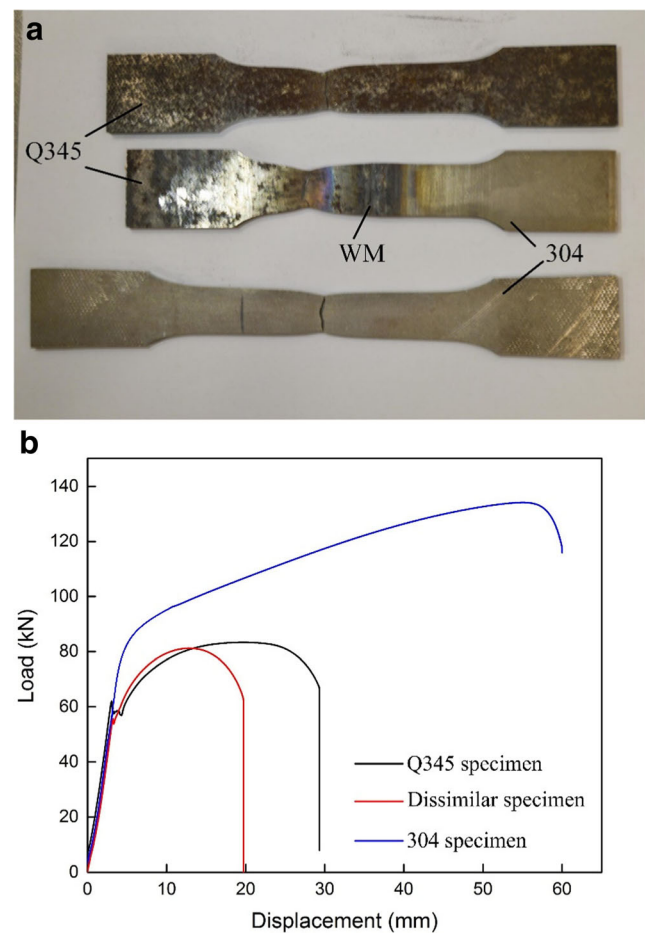
Fig. 11 Microhardness distribution on weld joints

Fig. 12 Results of tensile test. a Tensile test specimens. b Tensile curves of BMs and dissimilar specimen

different welding current. The weld metal is of conspicuous high hardness up to $393HV_1$ on average (510A), while the base metal hardnesses are 154 HV_1 in Q345 and 191 HV_1 in 304, respectively. Material hardness is mainly influenced by element components, phase compositions, and grain size. As mentioned above, the weld metal consists of lath martensite and retained austenite, which leads to the high hardness. HAZ of Q345 shows an increasing hardness as it is close to the fusion line. In welding of austenite steel and perlite steel, obvious carbon migration phenomenon can be observed near the interface of perlite steel and weld metal as shown in Fig. 8a [22], causing a carbon-enriched zone in weld side and a decarburization zone in Q345 side. Even so, the grain growth and the corresponding hardenability increase are dominant factors for the hardness increase. Though the HAZ grain size grows in the welding process, element migration also makes a great difference in structure hardening. Hardness of 304 base metal is no obvious change, corresponding to the microstructure mentioned earlier.

3.4 Tensile properties

Results of tensile test are shown in Fig. 12. Dissimilar specimen and BM specimens are shown in Fig.12a. Considering the fracture position of the dissimilar specimen, failures are obtained in the Q345 side, which indicates a good strength of the weld metal. Tensile curves are shown in Fig.12b. As we can see, peak loads of Q345 BM and 304 BM are 83.3 and 134.2 kN, equivalent to 416.5 and 671 MPa of ultimate tensile strength (UTS) respectively. And the peak load of dissimilar specimen is 81.2 kN and equivalent to UTS of 406 MPa. Therefore, the strength of the weldment reaches 97.5%

of that of the Q345 BM, and the K-TIG dissimilar joint quality is relatively high in strength. In addition, three specimens show different ductility; hence, the DIC results are shown to analyze the deformation and elastic-plastic properties.

Figure 13 shows dissimilar specimen's deformation in different strain condition, and from the test begin to the end as in a to g. The area of speckle is divided into three areas, 304, WM, and Q345 respectively. As shown in Fig. 13, elongation of the 304 and WM areas is not obvious, and the Q345 area has a large deformation especially at neck. At first, both base metals are deformed with the load. And, because yield strength of 304 steel is a little higher than that of Q345's, the deformation of 304 steel will tend to stop when Q345 starts to yield. At the same time, the load is confined in a relatively lower level by the ultimate strength of Q345 steel, resulting in a slower deformation of 304 steel. By calculation, the elongation is 2.56% for 304, 8.65% for WM, and 41.01% for Q345. As we know above, the peak load of dissimilar specimen is 81.2 kN, and in this load, 304 BM only has a slight deformation as shown in Fig.12b. Therefore, though the 304 BM has a
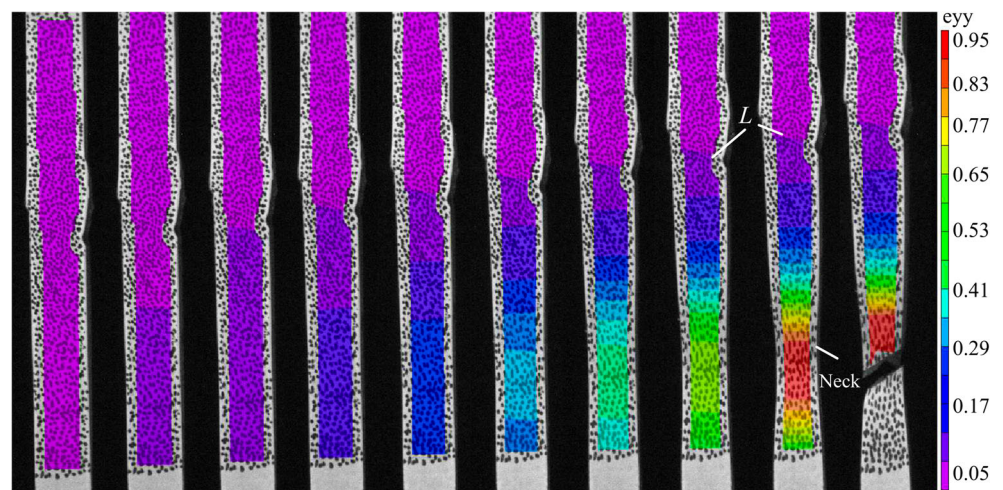
Fig. 13 Deformation of weld joint in different strain condition

a	b	c	d	e	f	g

| Strain | 0% | 5.12% | 7.76% | 12.05% | 15.51% | 22.44% | -- |
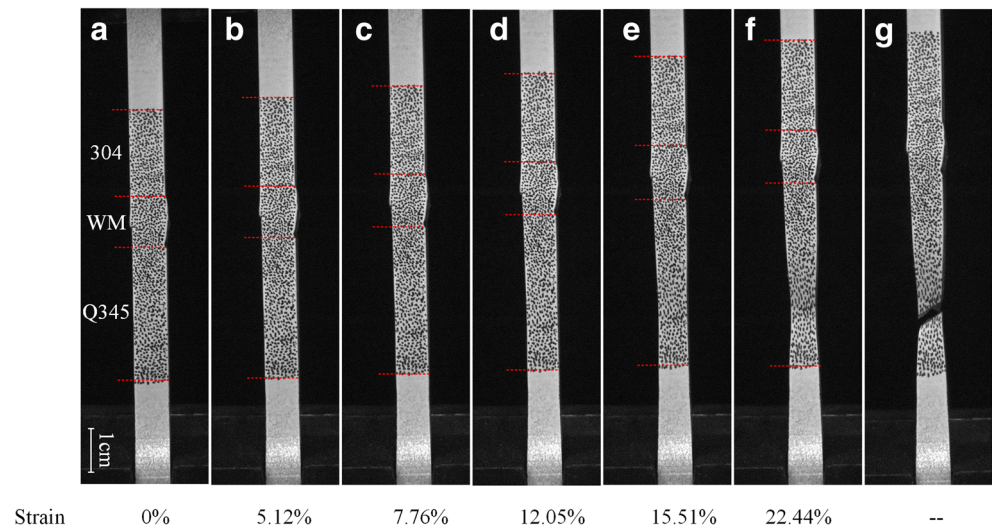
good ductility, it contributes little to dissimilar joint ductility.

Figure 14 shows the local strain distribution in the whole test. The legend, eyy, represents the vertical strain of the material. As test go on, local strain accumulates in the neck gradually, leading to final fracture. The L line in Fig. 14 shows a tilted gradient along the fusion line. This can attribute to the large difference in microstructure between WM and HAZ of Q345. Lath martensite in WM is of high strength and is hard to deform, and strength of Widmanstatten structure and proeutectoid ferrite in Q345 is much lower, resulting in an obvious boundary. Additionally, the neck is located in Q345 BM far away from the weld. This is because, on the one hand, carbon and other elements accumulate to the fusion line as mentioned above, causing a hardening area close to the fusion line; on the other hand, the existence of microcrack in BM forms stress concentration areas, making the fracture easier.

4 Conclusions

Eight-millimeter-thick AISI 304 stainless steel and Q345 low-alloy steel were welded by keyhole TIG in the study. The following conclusions can be made.

(1) K-TIG welding can be applied to mid-thickness dissimilar steels with a relatively high weld speed (300–400 mm/min) in single pass. Weld current process windows can reach to 50A, and WF increases as weld current. However, WB have no obvious increase because of the keyhole stability.

(2) Deviation between tungsten and center line (DTC) should be precisely controlled because of the arc blow. A non-negative value (not more than 2 mm) of DTC can avoid weld pool collapse or incomplete fusion.

(3) Weld metal consists of lath martensite and retained austenite. Widmanstatten structure and proeutectoid ferrite

Fig. 14 Local strain distribution of weld joint in tensile test by DIC system

formed in HAZ of Q345 BM. And HAZ of 304 BM is relatively narrow, with no obvious grain growth.

(4) Microhardness of WM is higher than BMs, which is attributed to the formation of martensite. The strength of weld is almost the same as that of the Q345 base metal, and the elongation of weld is slightly less than that of the Q345 base metal. The element accumulation and microcracks in base metal results in a fracture position far from weld.

References

1. Jarvis BL, Ahmed NU (2000) Development of keyhole mode gas tungsten arc welding process. Sci Technol Weld Join 5(1):21–1718
2. Liu ZM, Fang YX, Cui SL, Luo Z, Liu WD, Liu ZY, Jiang Q, Yi S (2016) Stable keyhole welding process with K-TIG. J Mater Process Technol 238:65–72
3. Feng Y, Luo Z, Liu Z, Li Y, Luo Y, Huang Y (2015) Keyhole gas tungsten arc welding of AISI 316l stainless steel. Mater Des 85:24–31
4. Fan WF, Ao SS, Huang YF, Liu WD, Li Y, Feng YQ, Luo Z, Wu B (2017) Water cooling keyhole gas tungsten arc welding of HSLA steel. Int J Adv Manuf Technol 6:1–10
5. Fang YX, Liu ZM, Cui SL, Zhang Y, Qiu JY, Luo Z (2017) Improving q345 weld microstructure and mechanical properties with high frequency current arc in keyhole mode TIG welding. J Mater Process Technol 250:280–288
6. Paventhan R, Lakshminarayanan PR, Balasubramanian V (2011) Fatigue behaviour of friction welded medium carbon steel and austenitic stainless steel dissimilar joints. Mater Des 32(4):1888–1894
7. Özdemir N (2005) Investigation of the mechanical properties of friction-welded joints between AISI 304l and AISI 4340 steel as a function rotational speed. Mater Lett 59(19–20):2504–2509
8. Pouraliakbar H, Mohsen H, Kokabi AH, Nazari A (2014) Designing of ck45 carbon steel and aisi 304 stainless steel dissimilar welds. Mater Res 17(1):106–114
9. Chen S, Zhai Z, Huang J, Zhao X, Xiong J (2016) Interface microstructure and fracture behavior of single/dual-beam laser welded steel-al dissimilar joint produced with copper interlayer. Int J Adv Manuf Technol 82(1–4):631–643
10. Li G, Huang J, Wu Y (2015) An investigation on microstructure and properties of dissimilar welded Inconel 625 and sus 304 using high-power co 2, laser. Int J Adv Manuf Technol 76(5–8):1203–1214
11. Romoli L, Rashed CAA (2015) The influence of laser welding configuration on the properties of dissimilar stainless steel welds. Int J Adv Manuf Technol 81(1–4):563–576
12. Sun Z, Ion JC (1995) Laser welding of dissimilar metal combinations. J Mater Sci 30(17):4205–4214
13. Torkamany MJ, Sabbaghzadeh J, Hamedi MJ (2012) Effect of laser welding mode on the microstructure and mechanical performance of dissimilar laser spot welds between low carbon and austenitic stainless steels. Mater Des 34:666–672
14. GB 2651 (2008) Tensile test methods on welded joints, general administration of quality supervision, inspection and quarantine of the People's Republic of China, China National Standardization Management Committee
15. Peters, W. H., & Ranson, W. F. (1982). Digital imaging techniques in experimental stress analysis. Environmental jurisprudence in India. Kluwer Law International
16. Chu TC, Ranson WF, Sutton MA (1985) Applications of digital-image-correlation techniques to experimental mechanics. Exp Mech 25(3):232–244
17. Xu X, Su Y, Zhang Q (2017) Theoretical estimation of systematic errors in local deformation measurements using digital image correlation. Opt Lasers Eng 88:265–279
18. Reis RP, Souza MD, Scotti A (2011) Models, to describe plasma jet, arc trajectory, and arc blow formation in arc welding. Weld World 55(3–4):24–32
19. Sadeghian M, Shamanian M, Shafyei A (2014) Effect of heat input on microstructure and mechanical properties of dissimilar joints between super duplex stainless steel and high strength low alloy steel. Mater Des 60(8):678–684
20. Ashiq M, Dhekne P, Hamada AS, Sahu P, Mahato B, Minz RK, Chowdhury SG, Karjalainen LP (2017) Correlation of microstructure and texture in a two-phase high-Mn twinning-induced plasticity steel during cold rolling. Metall Mater Trans A:1–15
21. Kchaou Y, Haddar N, Hénaff G, Pelosin V, Elleuch K (2014) Microstructural, compositional and mechanical investigation of shielded metal arc welding (SMAW) welded superaustenitic UNS n08028 (alloy 28) stainless steel. Mater Des 63(21):278–285
22. Wu W, Hu S, Shen J (2015) Microstructure, mechanical properties and corrosion behavior of laser welded dissimilar joints between ferritic stainless steel and carbon steel. Mater Des (1980–2015) 65:855–861